Science AAAS

N_2 Reduction and Hydrogenation to Ammonia by a Molecular Iron-Potassium Complex

Meghan M. Rodriguez, *et al.*

Science **334**, 780 (2011);
DOI: 10.1126/science.1211906

This copy is for your personal, non-commercial use only.

If you wish to distribute this article to others, you can order high-quality copies for your colleagues, clients, or customers by clicking here.

Permission to republish or repurpose articles or portions of articles can be obtained by following the guidelines here.

The following resources related to this article are available online at www.sciencemag.org (this infomation is current as of November 12, 2011):

Updated information and services, including high-resolution figures, can be found in the online version of this article at:
http://www.sciencemag.org/content/334/6057/780.full.html

Supporting Online Material can be found at:
http://www.sciencemag.org/content/suppl/2011/11/10/334.6057.780.DC1.html

A list of selected additional articles on the Science Web sites **related to this article** can be found at:
http://www.sciencemag.org/content/334/6057/780.full.html#related

This article **cites 65 articles**, 5 of which can be accessed free:
http://www.sciencemag.org/content/334/6057/780.full.html#ref-list-1

This article appears in the following **subject collections:**
Chemistry
http://www.sciencemag.org/cgi/collection/chemistry

Science (print ISSN 0036-8075; online ISSN 1095-9203) is published weekly, except the last week in December, by the American Association for the Advancement of Science, 1200 New York Avenue NW, Washington, DC 20005. Copyright 2011 by the American Association for the Advancement of Science; all rights reserved. The title *Science* is a registered trademark of AAAS.

and then dosing TFAP on the modified surface with similar coverages, pro-*R* excesses of up to 16 ± 3% are observed. This behavior can be explained simply by low barrier rotation of the trifluoroacetyl group followed by preferential capture of pro-*R* TFAP to form diastereomeric complexes at free binding sites around the ethylamine group of the modifier. The observed symmetry breaking is a direct manifestation of the action of (*R*)-NEA as a chiral modifier of the Pt(111) surface.

The previous lack of direct information on modifier-substrate stereodirecting interactions has been the major roadblock in the comprehension and optimization of chirally modified heterogeneous asymmetric catalysts. As this study demonstrates, efficient stereodirection occurs through subtle energy differences in the presence of stronger ones, including chemisorption bonding. It is extraordinarily difficult to identify the origin of these differences, and their relative importance, in the absence of direct measurements. The combination of STM and DFT used here to describe chirality transfer preorganization in terms of regiospecific prochiral ratios is a key step forward. It can serve as a basis for profound studies of the kinetic relevance of individual submolecular sites as well as for studies of the stereodynamics of heterogeneous asymmetric induction. Our model-free analysis suggests that for the NEA-TFAP pair a higher enantiomeric excess could be achieved by molecular design to limit the chiral pocket to one binding site, rather than the multiple sites observed. Efforts could be directed toward blocking the counterproductive β site and/or favoring chemisorption of NEA-1 over the less-selective NEA-2 conformer. In future work, STM/DFT-guided asymmetric catalyst design could be applied to other modifier substrate pairs and a broader range of reactions.

References and Notes

1. G. Kyriakou, S. K. Beaumont, R. M. Lambert, *Langmuir* **27**, 9687 (2011).
2. M. Forster, M. S. Dyer, M. Persson, R. Raval, *Top. Catal.* **54**, 13 (2011).
3. A. J. Gellman, *ACS Nano* **4**, 5 (2010).
4. A. G. Trant, C. J. Baddeley, *J. Phys. Chem. C* **115**, 1025 (2011).
5. K. H. Ernst, *Orig. Life Evol. Biosph.* **40**, 41 (2010).
6. H.-U. Blaser, M. Studer, *Acc. Chem. Res.* **40**, 1348 (2007).
7. M. Heitbaum, F. Glorius, I. Escher, *Angew. Chem. Int. Ed.* **45**, 4732 (2006).
8. E. Orglmeister, T. Mallat, A. Baiker, *Adv. Synth. Catal.* **347**, 78 (2005).
9. J. M. Bonello, F. J. Williams, R. M. Lambert, *J. Am. Chem. Soc.* **125**, 2723 (2003).
10. Q. Chen, N. V. Richardson, *Nat. Mater.* **2**, 324 (2003).
11. S. Weigelt *et al.*, *Nat. Mater.* **5**, 112 (2006).
12. A. Kühnle, T. R. Linderoth, B. Hammer, F. Besenbacher, *Nature* **415**, 891 (2002).
13. L. Ning, S. Haq, G. R. Darling, R. Raval, *Angew. Chem. Int. Ed.* **40**, 7613 (2007).
14. M. Lingenfelder *et al.*, *Angew. Chem. Int. Ed.* **46**, 4492 (2007).
15. S. Blankenburg, W. G. Schmidt, *Phys. Rev. Lett.* **99**, 196107 (2007).
16. L. Burkholder, M. Garvey, M. Weinert, W. T. Tysoe, *J. Phys. Chem. C* **115**, 8790 (2011).
17. V. Demers-Carpentier *et al.*, *J. Phys. Chem. C* **115**, 1355 (2011).
18. R. R. Knowles, E. N. Jacobsen, *Proc. Natl. Acad. Sci. U.S.A.* **107**, 20678 (2010).
19. A. Zehnacker, M. A. Suhm, *Angew. Chem. Int. Ed.* **47**, 6970 (2008).

Acknowledgments: This work was supported by a Natural Sciences and Engineering Research Council of Canada (NSERC) discovery grant, a Fonds Québécois de la Recherche sur la Nature et les Technologies (FQRNT) team grant, Canadian Foundation for Innovation (CFI) grants, and the FQRNT Centre in Green Chemistry and Catalysis (CCVC). This work was in part supported by the Lundbeck Foundation, the Danish Research Councils, and the Danish Center for Scientific Computing. V.D.-C. acknowledges an NSERC graduate student scholarship.

Supporting Online Material
www.sciencemag.org/cgi/content/full/334/6057/776/DC1
Materials and Methods
SOM Text
Figs. S1 to S19
Tables S1 to S4
References (*20–38*)
Movie S1

20 May 2011; accepted 19 September 2011
10.1126/science.1208710

N_2 Reduction and Hydrogenation to Ammonia by a Molecular Iron-Potassium Complex

Meghan M. Rodriguez,[1] Eckhard Bill,[2] William W. Brennessel,[1] Patrick L. Holland[1]*

The most common catalyst in the Haber-Bosch process for the hydrogenation of dinitrogen (N_2) to ammonia (NH_3) is an iron surface promoted with potassium cations (K^+), but soluble iron complexes have neither reduced the N-N bond of N_2 to nitride (N^{3-}) nor produced large amounts of NH_3 from N_2. We report a molecular iron complex that reacts with N_2 and a potassium reductant to give a complex with two nitrides, which are bound to iron and potassium cations. The product has a Fe_3N_2 core, implying that three iron atoms cooperate to break the N-N triple bond through a six-electron reduction. The nitride complex reacts with acid and with H_2 to give substantial yields of N_2-derived ammonia. These reactions, although not yet catalytic, give structural and spectroscopic insight into N_2 cleavage and N-H bond-forming reactions of iron.

The Haber-Bosch process is a large-scale method for catalytic reduction of dinitrogen (N_2) with dihydrogen (H_2) to give ammonia (NH_3). This process is vital for production of synthetic fertilizer, which is needed to produce food for the world's expanding population (*1*). Several metals catalyze the Haber-Bosch process (iron, ruthenium, osmium, uranium, and cobalt-molybdenum), but iron has received the most industrial and theoretical attention because of its hardiness and low cost (*2*–*4*). The most common iron catalyst is promoted by K^+ additives and was developed by Mittasch in 1910 (*2*). In the century since then, chemists have studied the nature of active iron and iron/potassium surfaces, as well as the kinetics of N_2 reduction (*3*). These studies have shown that iron is predominantly in the zero oxidation state in the catalyst. Importantly, the rate-limiting step of the catalytic process is N_2 chemisorption and N-N bond cleavage to give surface-bound nitrides (N^{3-}), which react with H_2 to form the N-H bonds in NH_3 (Fig. 1). However, many details of the bond-breaking and bond-forming steps are difficult to discern by using surface science techniques, for example, how many iron atoms are involved in the N-N dissociation step and whether the K^+ promoter interacts with N_2 during the N-N dissociation step (*4*). Similar uncertainties surround postulated mechanisms for N_2 reduction by nitrogenase enzymes, which have iron (in the +2 and +3 oxidation states) at their active sites (*5*, *6*).

Reactions of iron coordination compounds with N_2 are of interest because the products can shed light on Fe-N_2 interactions in atomic detail. Although the behavior of iron atoms in a coordination compound (where they have a positive formal charge) is inevitably different than the zero valent iron atoms on a metallic surface, coordination compounds are more amenable to detailed structural characterization. Unfortunately, iron coordination complexes are poor at reduc-

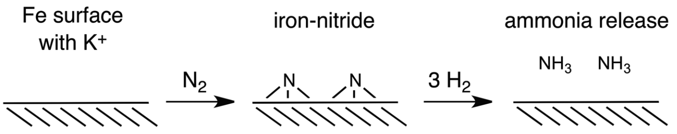

Fig. 1. Simplified scheme of the ammonia formation pathway in the Haber-Bosch process.

---

[1] Department of Chemistry, University of Rochester, Rochester, NY 14627, USA. [2] Max-Planck-Institut für Bioanorganische Chemie, Stiftstrasse 34-36, D-45470 Mülheim an der Ruhr, Germany.

*To whom correspondence should be addressed. E-mail: holland@chem.rochester.edu ing N_2 (*7*, *8*). Known Fe-N_2 complexes have not been observed to give iron-nitride products and produce little (if any) ammonia upon exposure to acids or H_2 (*9*–*13*). Here, we report an iron-potassium system that completely cleaves the N-N triple bond of N_2 to give a product with two nitride (N^{3-}) ligands derived from N_2. The N_2-derived nitride complex reacts with H_2 to give a substantial yield of ammonia. This work displays the structural characteristics of an iron-based N_2-cleaving system and suggests that cooperation between metal atoms helps to achieve N-N bond cleavage and N-H bond formation on iron.

Consistent with their low reactivity toward N-N bond cleavage, the N-N bonds in most mononuclear and dinuclear Fe-N_2 complexes are within 0.04 Å of the N-N distance in free N_2 (1.10 Å) (*7*, *8*). A few research groups have reported significant N-N bond weakening in iron-N_2 complexes by using bulky, electron-rich ligands with N or P donors (*14*–*16*). Our research has revealed that Fe-N_2 complexes with low-coordinate iron weaken the N-N bond to between 1.17 and 1.23 Å (*14*, *17*). The greatest weakening (N-N = 1.23 Å; $\nu_{N\text{-}N}$ = 1589 cm^{-1}) is in β-diketiminate complex $K_2[L^1FeNNFeL^1]$ {L^1 is $HC[C(^tBu)N(2,6\text{-}^iPr_2C_6H_3)]_2^-$, where ^{t}Bu is a *tert*-butyl group and ^{i}Pr indicates an isopropyl group; Fig. 2A}, which comes from treating L^1FeCl with potassium graphite (KC_8) under N_2 (*14*). Similar N-N weakening is observed in analogs containing the slightly less hindering L^2 {L^2 is $HC[C(Me)N(2,6\text{-}^iPr_2C_6H_3)]_2^-$, where Me is a methyl group; Fig. 2B}. The research reported here uses L^3 {L^3 is $MeC[C(Me)N(2,6\text{-}Me_2C_6H_3)]_2^-$; Fig. 2C), which is less sterically hindering by virtue of having methyl rather than isopropyl groups on the aryl rings. The new iron(II) chloride complex $[L^3Fe(\mu\text{-}Cl)]_2$ (**1**) can be prepared like earlier β-diketiminate–supported iron(II) chloride complexes (*18*, *19*).

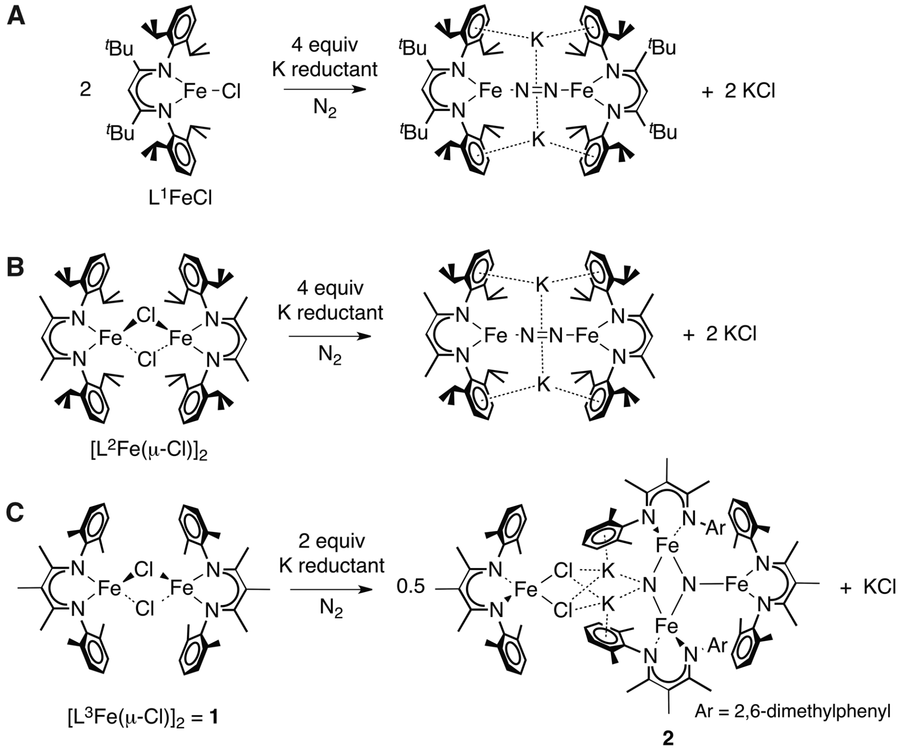

Fig. 2. Iron complexes with varying steric bulk give different N_2 products upon reduction by potassium (introduced as KC_8, potassium graphite). (**A**) Bulky ligand L^1 (*17*). (**B**) Bulky ligand L^2 (*14*).(**C**) Less bulky ligand L^3 (this work).

Mixing **1** with two molar equivalents of KC_8 in tetrahydrofuran (THF) under an atmosphere of N_2 gives a red-brown tetrairon bis(nitride) complex (**2**) (Fig. 2C). This product can be isolated as analytically pure crystals in 43% yield. The use of THF as reaction solvent is critical: Formation of **2** is not observed by proton nuclear magnetic resonance (^{1}H NMR) spectroscopy when the reaction is performed in other solvents such as pentane and toluene. No formation of **2** is observed when **1** is treated with KC_8 under an atmosphere of argon rather than N_2; instead, a mixture of unidentified products is evident. Use of $^{15}N_2$ gives an isotopically labeled product (see below), demonstrating that the nitrides originate from N_2. Solutions of purified **2** decompose to unidentified products with a half-life of 8 hours at 25°C in benzene-d_6, although crystalline samples of **2** suffer no apparent decomposition when stored for up to 1 month at –40°C.

X-ray crystallography shows the molecular structure of **2** (Fig. 3), which has a core of three iron centers (Fe1, Fe2, and Fe3) surrounding two bridging nitrogens. The N-N distance of 2.799(2) Å (number in parentheses indicates the estimated standard deviation in the final digit) indicates that there is no N-N bond; thus, six-electron reduction of N_2 has given two bridging nitrides (N^{3-}). One of the nitrides (N2) is attached to three irons, and the other (N1) bonds to two irons as well as two potassiums. Each potassium interacts with two chlorides and with a diketiminate aryl group through a π-cation interaction. A fourth iron center (Fe4) is bound to the chlorides and displays a pseudotetrahedral geometry. The Fe-N distances to the potassium-bound N1 are shorter than the Fe-N distances to the triply bridging N2, most likely from steric clashes between the three β-diketiminate ligands bound to Fe1, Fe2, and Fe3.

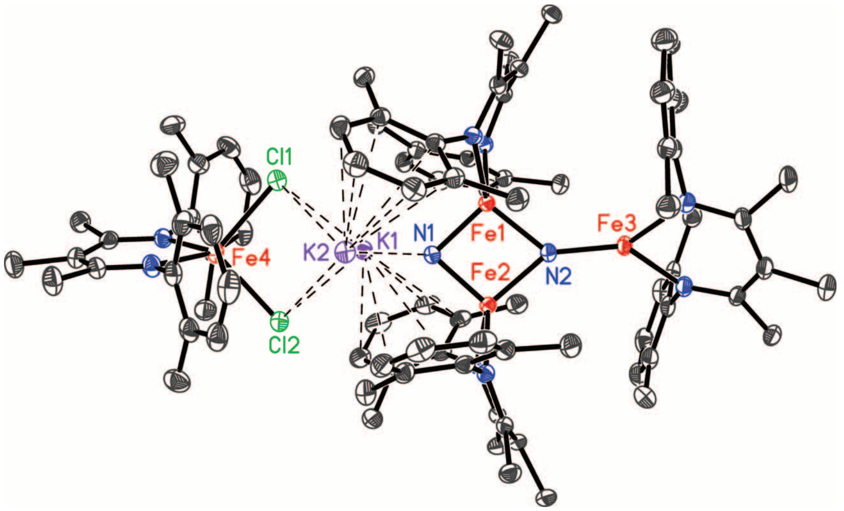

Fig. 3. Molecular structure of **2** using 50% probability ellipsoids. Hydrogen atoms and cocrystallized solvent molecules have been omitted for clarity. Selected bond lengths and angles are as follows: Fe1-N1, 1.812(2) Å; Fe1-N2, 1.906(2) Å; Fe2-N1, 1.809(2) Å; Fe2-N2, 1.918(2) Å; Fe3-N2, 1.832(2) Å; Fe1-Fe2, 2.4531(4) Å; N1-N2, 2.799(2) Å; Fe1-N1-Fe2, 85.27(7)°; Fe1-N2-Fe2, 79.79(7)°; Fe3-N2-Fe1, 135.9(1)°; Fe3-N2-Fe2, 143.6(1)°.

NMR spectroscopy suggests that the solution structure of **2** is similar to the solid-state structure. Fifteen paramagnetically shifted resonances are observed in the ^{1}H NMR spectrum of **2**, and the number and integrations of the resonances are consistent with C_{2v} symmetry in solution, with

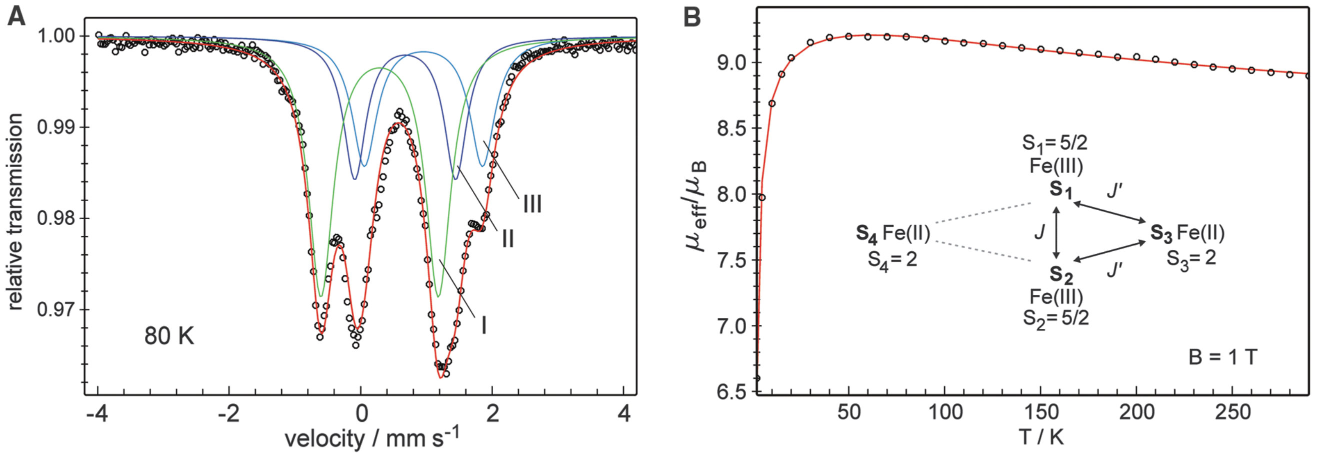

Fig. 4. (**A**) Zero-field Mössbauer spectrum of solid **2** at 80 K. The red line is a superposition of the three Lorentzian doublets I, II, and III with intensity ratio 2:1:1. (**B**) Temperature dependence of the effective magnetic moment of **2** measured at magnetic induction (*B*) = 1 T. The solid line represents a spin Hamiltonian simulation with four spins and two exchange coupling constants, as indicated in the inset.

equivalent β-diketiminate ligands on Fe1 and Fe2. The solubility of **2** in nonpolar solvents like hexane and diethyl ether also suggests that the potassium cations are held tightly within the structure in solution.

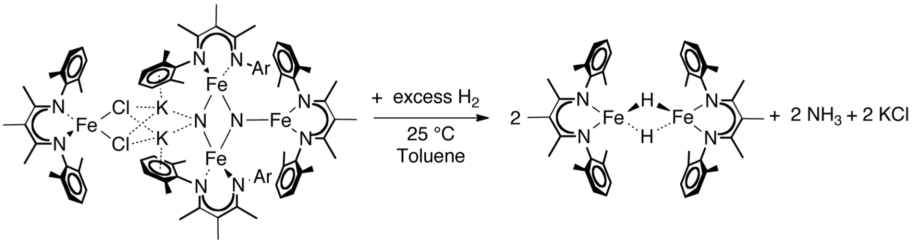

Fig. 5. The reaction of **2** with H_2 produces NH_3 in 42 ± 2% yield.

The zero-field Mössbauer spectrum of a crystalline sample of **2** at 80 K (Fig. 4A) indicates three different iron environments, and the isomer shifts (δ) can be used to gauge their oxidation states by comparison to literature values (table S2). The isomer shift for subspectrum I (δ = 0.29 mm/s) is similar to those for high-spin Fe^{3+} sites in nitride and sulfide clusters (*20*–*22*). Subspectrum I has twice the intensity of the other subspectra, indicating that the equivalent Fe1 and Fe2 sites are high-spin Fe^{3+}. Subspectra II and III of **2** exhibit higher isomer shifts that are typical of high-spin Fe^{2+} sites. The Mössbauer parameters of subspectrum II (δ = 0.68 mm/s, ΔE_Q = 1.54 mm/s, where ΔE_Q is the quadrupole splitting) resemble those for the planar three-coordinate Fe^{2+} complexes L^{1}FeNHR (R is *p*-tolyl and *tert*-butyl), which have a similar environment as Fe3 (*23*). Subspectrum III shows parameters (δ = 0.96 mm/s, ΔE_Q = 1.80 mm/s) that are typical of quasi-tetrahedral high-spin Fe^{2+} compounds such as L^{2}Fe(μ-Cl)$_2$Li(ether)$_2$ (*24*). Comparison of the Fe-N(diketiminate) bond lengths in Fe4 to Fe^{2+} and Fe^{3+} compounds of L^3 also suggests a Fe^{2+} assignment for Fe4 (table S1). Thus, signal II can be confidently assigned to Fe3, and signal III to Fe4.

The assignments of high-spin Fe^{3+} for Fe1 and Fe2, and of high-spin Fe^{2+} for Fe3 and Fe4, are corroborated by the magnetic properties of solid **2**. The temperature dependence of the effective magnetic moment (Fig. 4B) can be simulated by using the spin topology indicated in the Fig. 4B inset. The triad made up of Fe1, Fe2, and Fe3 has ground state S_{123} = 3 because of dominant antiferromagnetic coupling of S_3 to both S_1 and S_2, which is stronger than the antiferromagnetic coupling between S_1 and S_2. The effective magnetic moment of **2** fits the superposition of the moments from S_{123} and from the uncoupled ferrous Fe4 site, with $\mu_{eff}^2 = \mu_{eff,123}^2 + \mu_{eff,4}^2$ (*25*).

The yield of ammonia derived from N_2 upon addition of acid is a measure of N_2 activation. Some carefully designed molybdenum compounds can produce ammonia catalytically with acids (*26*, *27*), but previous Fe-N_2 complexes have not given more than 10% yield of ammonia, indicating weak activation of coordinated N_2 (*7*–*13*, *28*). In contrast, treatment of a THF solution of **2** with 100 molar equivalents of ethereal HCl gives ammonia (present as its conjugate acid, NH_4^+) in 82 ± 4% yield (±range). Control experiments with other complexes of L^3, or N_2 complexes of other diketiminate ligands, give no detectable amount of ammonia. Reaction of **2** with acid to give a high yield of ammonia demonstrates that the N-N bond is completely cleaved and that the nitrides are nucleophilic.

The reaction of **1** with KC_8 may be carried out under an atmosphere of $^{15}N_2$ to generate isotopically labeled samples of **2**-^{15}N. Purified **2**-^{15}N reacts with acid to form $^{15}NH_4^+$, which may be identified from its characteristic 1:1 doublet in the ^{1}H NMR spectrum. An analogous reaction with unlabeled **2** and excess acid shows a 1:1:1 triplet for $^{14}NH_4Cl$. These labeling studies verify that the nitrides in **2** come from N_2 and that the ammonia comes from these nitrides.

Iron-nitride complexes typically have terminal and bridging nitrides that are derived from reactive N sources such as N_3^- (*22*). Recently reported iron clusters with triply bridging nitrides used N(SnMe$_3$)$_3$ as the nitride source (*20*, *21*). The iron system reported here generates nitrides instead from the six-electron reduction of N_2, and we suggest two possible explanations for its N_2-reducing ability. First is the influence of the K$^+$ generated from reduction of the Fe^{2+} ions in **1** by potassium graphite. On metallic iron-potassium catalysts, it is thought that surface K$^+$ promotes N_2 dissociation by pulling electron density toward the surface iron atoms (*3*). The interaction of K$^+$ with the nitrides in our synthetic compound suggests that direct K$^+$-N_2 interactions could also be considered as contributors to the potassium promotion effect. Second, because more-hindered L^{1}Fe and L^{2}Fe gave bimetallic Fe_2N_2 species without N-N cleavage (*14*, *17*) and the less-protected L^{3}Fe gives N-N cleavage in **2**, it is likely that the ability of more metal atoms to simultaneously access the N_2 molecule is important for N_2 cleavage. From a thermodynamic perspective, it is reasonable that the formation of more iron-nitrogen bonds can better balance the energetic cost of breaking the N-N triple bond. On iron metal, the surfaces that are most active for N_2 reduction are those with sites that expose subsurface atoms (*29*). N_2 bound at such a site may interact in a cooperative fashion with several iron atoms to facilitate N-N cleavage, as suggested by computational studies (*30*).

It is most relevant to the Haber-Bosch process to show that formation of ammonia from an iron nitride is possible through reaction with dihydrogen. When electropositive early transition metal complexes cleave N_2 to metal-nitride complexes, the products rarely react with H_2 to give ammonia. In the best previous example, reaction of free H_2 with a well-characterized N_2-derived zirconium nitride complex formed ammonia in 10 to 15% yield (*31*). Shaking a solution of **2** in toluene with 1 atm of H_2 at room temperature for 6 hours produces NH_3 in 42 ± 2% yield (Fig. 5). The main iron-containing product of the reaction of **2** with H_2 is $[L^3Fe(\mu\text{-}H)]_2$, which is generated in 43 ± 4% yield as shown by ^1H NMR spectroscopy. Thus, the soluble molecular iron system described here is capable of performing both N_2 cleavage and hydrogenation.

How do these results relate to the Mittasch iron catalyst that is used for the Haber-Bosch process? It is likely that potassium reduction of the Fe^{2+} precursor **1** leads to a high-spin Fe^{1+} intermediate, by analogy to related complexes (*14*). The metal in a low oxidation state can donate charge to N_2 that weakens the N-N bond, and this effect is heightened by a low coordination number at the metal (*14*). Surface irons on the Mittasch catalyst also have a low oxidation state and low coordination number (*3*), suggesting a potential parallel. In a second commonality, a molecule of N_2 may react simultaneously with multiple unsaturated iron atoms during the formation of **2** and on an iron surface. Nitrogenase uses a cluster of iron atoms to reduce N_2 (*5*, *6*), suggesting that cooperativity may be important in biological N_2 reduction as well. Thirdly, potassium has a beneficial effect on N-N bond cleavage by the Mittasch catalyst, perhaps through a direct interaction between potassium and nitrogen like that observed in **2**. Lastly, we suggest that the presence of a three-coordinate iron atom near the nitrides may enable iron to split H_2 at the unsaturated site and form N-H bonds without extensive reorganization. Further studies will test these hypotheses derived from the structure and behavior of **2**.

References and Notes

1. V. Smil, *Sci. Am.* **277**, 76 (1997).
2. A. Mittasch, *Geschichte der Ammoniaksynthese* (Verlag Chemie, Weinheim, Germany, 1951).
3. R. Schlögl, in *Handbook of Heterogeneous Catalysis*, G. Ertl, H. Knözinger, F. Schüth, J. Weitkamp, Eds. (Wiley-VCH, Weinheim, Germany, ed. 2, 2008), vol. 5, pp. 2501–2575.
4. A. Hellman *et al.*, *J. Phys. Chem. B* **110**, 17719 (2006).
5. B. K. Burgess, D. J. Lowe, *Chem. Rev.* **96**, 2983 (1996).
6. B. M. Hoffman, D. R. Dean, L. C. Seefeldt, *Acc. Chem. Res.* **42**, 609 (2009).
7. J. L. Crossland, D. R. Tyler, *Coord. Chem. Rev.* **254**, 1883 (2010).
8. N. Hazari, *Chem. Soc. Rev.* **39**, 4044 (2010).
9. G. N. Schrauzer, T. D. Guth, *J. Am. Chem. Soc.* **98**, 3508 (1976).
10. A. Hills, D. L. Hughes, M. Jimenez-Tenorio, G. J. Leigh, A. T. Rowley, *J. Chem. Soc. Dalton Trans.* **1993**, 3041 (1993).
11. T. A. George, D. J. Rose, Y. Chang, Q. Chen, J. Zubieta, *Inorg. Chem.* **34**, 1295 (1995).
12. D. A. Hall, G. J. Leigh, *J. Chem. Soc. Dalton Trans.* **1996**, 3539 (1996).
13. J. D. Gilbertson, N. K. Szymczak, D. R. Tyler, *J. Am. Chem. Soc.* **127**, 10184 (2005).
14. J. M. Smith *et al.*, *J. Am. Chem. Soc.* **128**, 756 (2006).
15. T. A. Betley, J. C. Peters, *J. Am. Chem. Soc.* **126**, 6252 (2004).
16. W. A. Chomitz, J. Arnold, *Chem. Commun.* **2007**, 4797 (2007).
17. J. M. Smith *et al.*, *J. Am. Chem. Soc.* **123**, 9222 (2001).
18. N. A. Eckert, J. M. Smith, R. J. Lachicotte, P. L. Holland, *Inorg. Chem.* **43**, 3306 (2004).
19. Materials and methods are available as supporting online material (SOM) on *Science* Online.
20. M. V. Bennett, S. Stoian, E. L. Bominaar, E. Münck, R. H. Holm, *J. Am. Chem. Soc.* **127**, 12378 (2005).
21. M. V. Bennett, R. H. Holm, *Angew. Chem. Int. Ed.* **45**, 5613 (2006).
22. Additional references may be found in the SOM.
23. H. Andres *et al.*, *J. Am. Chem. Soc.* **124**, 3012 (2002).
24. S. A. Stoian, J. M. Smith, P. L. Holland, E. Münck, E. L. Bominaar, *Inorg. Chem.* **47**, 8687 (2008).
25. The *g* values were fixed to $g = 2$ for the sake of unambiguity except for g_4, which was allowed to vary to 2.49 in order to match exactly the experimental values. See SOM for details and other fit values.
26. D. V. Yandulov, R. R. Schrock, *Science* **301**, 76 (2003).
27. K. Arashiba, Y. Miyake, Y. Nishibayashi, *Nat. Chem.* **3**, 120 (2011).
28. The yields given here are per nitrogen atom of N_2, in order to accurately reflect the fate of the two nitrogen atoms. In previous papers with mononuclear iron-N_2 complexes, the yield of NH_3 is typically calculated per iron atom.
29. D. R. Strongin, J. Carrazza, S. R. Bare, G. A. Somorjai, *J. Catal.* **103**, 213 (1987).
30. J. J. Mortensen, L. B. Hansen, B. Hammer, J. K. Nørskov, *J. Catal.* **182**, 479 (1999).
31. J. A. Pool, E. Lobkovsky, P. J. Chirik, *Nature* **427**, 527 (2004).

Acknowledgments: This work was supported by a grant from NIH (GM-065313). We thank C. Scarborough and R. Cowley for valuable discussions. Materials and methods are available as supporting material on *Science* Online. Crystallographic data for **2** (two independent structures with different solvents of crystallization), L^3FeCl_2, L^3FeCl_2K(18-crown-6), and $[L^3FeH]_2$ have been deposited with the Cambridge Crystallographic Data Centre with deposition numbers CCDC 836870 to 836874.

Supporting Online Material

www.sciencemag.org/cgi/content/full/334/6057/780/DC1
Materials and Methods
SOM Text
Figs. S1 to S3
Tables S1 and S2
References (*32–74*)

29 July 2011; accepted 20 September 2011
10.1126/science.1211906

Lithospheric Thinning Beneath Rifted Regions of Southern California

Vedran Lekic,* Scott W. French,† Karen M. Fischer

The stretching and break-up of tectonic plates by rifting control the evolution of continents and oceans, but the processes by which lithosphere deforms and accommodates strain during rifting remain enigmatic. Using scattering of teleseismic shear waves beneath rifted zones and adjacent areas in Southern California, we resolve the lithosphere-asthenosphere boundary and lithospheric thickness variations to directly constrain this deformation. Substantial and laterally abrupt lithospheric thinning beneath rifted regions suggests efficient strain localization. In the Salton Trough, either the mantle lithosphere has experienced more thinning than the crust, or large volumes of new lithosphere have been created. Lack of a systematic offset between surface and deep lithospheric deformation rules out simple shear along throughgoing unidirectional shallow-dipping shear zones, but is consistent with symmetric extension of the lithosphere.

During the break-up of a continental tectonic plate, the lithosphere thins, weakens, ruptures, and is replaced by new oceanic lithosphere. What enables this process has been widely debated, with contrasting views of crustal and mantle rheology, strain rate distribution (*1*–*8*), and the roles of melting (*7*, *8*), asthenospheric upwelling (*4*), and sedimentation (*6*–*8*). Prior constraints on the kinematics and dynamics of rifting have almost exclusively been provided by surface geologic and geochemical observations combined with geophysical imaging of the crust. We investigate the behavior of the mantle lithosphere during rifting by imaging its lower boundary at a geologically relevant length-scale.

In Southern California, extension followed the cessation of subduction ~30 million years ago (Ma) within the Continental Borderland region and continues beneath the Gulf of California and the Salton Trough (*9*). In the east, wide-mode rifting (*1*) occurs within the Basin and Range province. Excellent broadband station coverage provided by the Southern California Seismic Network, the Anza Network, and the Earthscope USArray (Fig. 1A) also make Southern California well suited for seismic imaging of the lithosphere. However, although tomographic models of upper-mantle structure abound (*10*, *11*), tomography cannot directly image a velocity discontinuity such as the lithosphere-asthenosphere boundary (LAB), and methods more sensitive to mantle discontinuities have not yet mapped lithospheric thickness at the scale of surface geologic blocks (*12*–*14*).

Department of Geological Sciences, Brown University, Providence, RI 02912, USA.

*To whom correspondence should be addressed. E-mail: vedran_lekic@brown.edu

†Present address: Berkeley Seismological Laboratory, University of California, Berkeley, CA 94720, USA.